



Adsorptive properties of biochar derived from biorefinery industry for basic dye removal

Yassine Bentahar¹ · Claire Lomenech¹ · Alice Mija² · Ed de Jong³ · Erik Bonjour⁴ · Patrick Jame⁴ · Charlotte Hurel¹

Received: 15 July 2022 / Revised: 7 October 2022 / Accepted: 10 October 2022 / Published online: 15 October 2022
© The Author(s), under exclusive licence to Springer-Verlag GmbH Germany, part of Springer Nature 2022

Abstract

The aim of this work was to investigate the use of biorefinery industry by-products such as humins as adsorbents for methylene blue (MB). After thermal treatment, these by-products are called biochars. Three biochars were used as adsorbents for MB removal: (i) a biochar obtained after thermal treatment of humins (called raw biochar), (ii) a biochar obtained after NaOH treatment of the biochar from (i) (called biochar-OH), (iii) a biochar obtained after mixing humins with lignin, this mixture being then submitted to the same thermal treatment than (i) (called humins-lignin biochar). Structural characterization was done using ATR-FTIR, BET surface area analysis, and scanning electron microscopy (SEM). An elemental analysis was conducted to determine C, H, N, S, and O content in samples. Adsorption experiments were carried out as a function of time, pH, different background electrolytes (NaNO₃ and CaCl₂), and initial MB concentration. Kinetics data showed a good compatibility of all adsorbents with the pseudo-second-order model. The affinity of MB for biochar increased noticeably with the increase in pH, particularly for biochar-OH and humins-lignin biochar. Both the NaNO₃ and CaCl₂ background electrolytes had a negative effect on adsorption processes, and Ca²⁺ and Na⁺ acted as competitor ions with MB on the surface. The Langmuir model was more suitable for biochar-OH and humins-lignin biochar, whereas neither the Langmuir nor the Freundlich isotherms fitted experimental results for raw biochar due to its very low adsorption capacity. The maximum adsorption capacity predicted by the Langmuir model allowed us to establish the following classification of biochars: biochar-OH > humins-lignin biochar > > > raw biochar. Modifications of the surface had a positive impact on the adsorption capacity due to the additional available functional groups incorporated into the surface through lignin enrichment and the clean-up of blocked pores through NaOH treatment. Furthermore, formation of macropores on biochar-OH through the NaOH treatment created additional adsorption sites and probably promoted the adsorption of MB via a pore-filling mechanism.

Keywords Humins · Lignin · Pseudo-second-order model · Surface modification · Langmuir model · Functional groups

1 Introduction

Waste management has become a global challenge faced by both developed and developing countries. Technology progress and population growth in the last decades have led to the generation of massive amounts of waste and the expansion of landfill sites. Hence, the necessity has become urgent to develop an efficient strategy to reduce the negative impact of waste (or of so-called by-products) on the environment. In this context, numerous studies have focused on the valorization of by-products that stem from various sectors and their conversion into value-added products [1–4].

Valorization of the waste stream produced by the biorefinery industry is considered a promising means of producing valuable polymeric materials. In the last few decades, the interest in biorefinery has been renewed, particularly for the

The authors declare that this work is not submitted to another journal.

✉ Yassine Bentahar
bentaharyassine@gmail.com

¹ Institut de Physique de Nice (INPHYNI), Université Côte d'Azur, 06108 Nice, France

² Institut de Chimie de Nice (ICN), Université Côte d'Azur, 06108 Nice, France

³ Avantium Renewable Polymers B.V, Zekeringstraat 29, 1014 BV Amsterdam, The Netherlands

⁴ Institut Des Sciences Analytiques (ISA), Université Lyon 1, CNRS UMR 5280, Université de Lyon, Lyon, France

conversion of agricultural side-products and agro-industrial/lignocellulosic waste into several platform chemicals such as levulinic acid, itaconic acid, and 5-hydroxymethyl furfural which subsequently can be transformed into fuel or fine chemicals [5–7]. However, the conversion process of carbohydrate and/or lignocellulosic-rich streams can be accompanied by the formation of humins or lignin solid residues. Humins, on the one hand, are released in high quantity and are considered the main drawback encountered in the conversion of carbohydrates into furanic intermediates [7]. Their production is inevitable when achieving commercial viable process conditions despite the many attempts to inhibit or at least minimize their formation [6, 8]. The attempt to valorize humins in added-value products could therefore have a positive impact on biorefinery activity [7]. To achieve this purpose, numerous methods have been applied including pyrolysis, gasification, wet oxidation, and hydrothermal degradation to produce valuable composites, oil, and syngas [7, 9]. Lignin, on the other hand, has been considered a low-value product and has traditionally been burned to generate power and energy for paper pulp as well as biorefinery plants. However, advances in biomass conversion technologies have led to the generation of more lignin than necessary to power biorefinery plants. Hence, the necessity has arisen to develop a new approach targeting the conversion of lignin into added-value products. The molecular structure of lignin which consists of a variety of functional groups explains its use in several industrial products such as food additives, pharmaceutical products, fuel, and textile [10–12].

Particular attention has been paid to the use of biorefinery by-products in wastewater treatment. The development of side-product-based biochar could contribute to both remediate wastewater and manage solid waste. An adequate synthesis route is fundamental to obtain a bio-sorbent with high porosity, a well-distributed pore size, and a reactive surface [13]. Also, chemical modification, coating of the biochar surface with a new additive, and the combination of biochars derived from different origins have been shown to enlarge the specific surface area and bring more oxygen functional groups to the surface [14, 15]. Numerous studies have reported that the combination via mechanical force of biochars derived from different feedstocks produced a multifunctional material with a large external and internal surface area and noticeably enhanced the adsorption capacity of organic compounds and dyes compared to a single biochar [16, 17]. The engineering of composite materials combining lignin with by-products such as chitin, cellulose, and red mud has been thoroughly investigated. The multi-component adsorbent resulting from this combination has shown an important ability to remove hydrophobic organic compounds, heavy metals, and dyes [18–20]. Biochar chemical modification generally requires additives such as acids,

bases, oxidizing agents, or organic or mineral compounds to improve the performance of biochar in removing pollutants. These additives significantly modify the surface reactivity by adding new reactive sites, increasing specific surface areas and porosity, which consequently improves contaminant removal [21–23]. Biochar surface treatment with sodium hydroxide has demonstrated a positive impact on the adsorption capacity, particularly of dye molecules. This modification enhances the porosity of biochar by creating several mesopores and macropores on the surface, in addition to providing an important quantity of oxygen functional groups on its structure, which improves the surface alkalinity and consequently the affinity for dye molecules [24, 25].

In this work, we investigated a biochar stemming from a biorefinery by-product (humins) generated during the acid-catalyzed dehydration (ACD) of sugars. A one-step thermal process was applied on this by-product in order to obtain a humin foam characterized by a complex molecular structure and macroporous morphology, with intrinsic self-foaming caused by its auto-cross-linking ability. Because of the physico-chemical properties of this humin foam, it has been suggested as an interesting recoverable material for environmental and energy applications (catalyst supports, adsorbents, and electrode materials) [6, 26]. In this study, a crushed humin foam was called biochar. We investigated its capacity to absorb methylene blue, a cationic hydrophilic dye. To improve the properties, the biochar surface was modified by (i) chemical treatment with sodium hydroxide and (ii) combination of humins with lignin (from paper industry waste) to produce a biochar. Avantium is currently constructing its flagship FDCA plant in the Netherlands so from 2024 onwards substantial amounts of humins will be produced [7]. Identifying value-added applications for this humin stream is therefore highly relevant.

The NaOH-treated biochar (biochar-OH) and the biochar obtained by the combination of humins with lignin (humins-lignin biochar) were characterized by FTIR, scanning electronic microscopy, specific surface area (BET) analysis, and CHNS elemental analysis. Adsorption experiments were subsequently carried out as a function of contact time, pH, and initial concentration of MB, in order to discover the possible interactions taking place during the adsorption processes. Experimental results were exploited using empirical methods and supported by the FTIR analysis carried out after adsorption of MB.

2 Materials and methods

2.1 Reagents

Methylene blue was purchased from Reactifs RAL. Nitric acid (HNO₃ 69%, Sigma Aldrich) and sodium hydroxide

(NaOH $\geq 97\%$, Alfa Aesar) were used to prepare diluted acidic and basic solutions for pH adjustment. The biochar was activated using a 3-M NaOH solution. All reagents were prepared using high-purity deionized water (resistivity 18.2 M Ω -cm, TOC $< 10 \mu\text{g}\cdot\text{L}^{-1}$) provided by Milli-Q Thermo Scientific.

Lignin and humins were kindly provided by Avantium Renewable Chemicals BV and used as received for the fabrication of the biochar and humins-lignin biochar.

2.2 Preparation of raw biochar and humins-lignin biochar

Raw biochar was prepared as follows: 25 g of biorefinery by-product was placed inside a Nabertherm K430/75 air-ventilated oven in a ceramic crucible. Due to the intrinsic chemical composition and structure of humins, auto-cross-linking reactions occur when submitted to heating under air, and the thermoset humins are produced with an autofoaming phenomenon. The temperature program has been optimized in a previous work in order that the obtained foam has reproducible and homogeneous properties (pore size, distribution, dimensions, evolution of viscosity, etc.) [6]. The humins-lignin biochar was prepared as follows: 10 g of humins was mixed with 5 g of lignin in a ceramic crucible. According to this previous work, to produce biochar and humins-lignin biochar a one-step temperature program was used: starting from 20 °C, the temperature was increased to 320 °C with a 10 °C min⁻¹ ramp rate. The samples were then kept at 320 °C for 20 min. Next, the oven temperature was set at 20 °C and the sample was allowed to cool down slowly. The samples were then crushed using a planetary ball mill (Retsch PM 100) for a grinding duration of 15 min, and the rotational speed was settled at 200 rpm. Automatic direction reversal was activated to avoid agglomerations. The powders obtained after crushing were sieved through a metallic sieve of 0.177 mm.

2.3 Chemical treatment of raw biochar by NaOH

Two grams of raw biochar powder was added to 300 mL of freshly prepared 3 M NaOH solution. This suspension was agitated for 4 h using a magnetic stirrer. The suspension was then vacuum-filtered through a filter paper and thoroughly washed with ultrapure water to eliminate the NaOH excess until the filtrate reached a neutral pH. The sample was dried for 24 h at 80 °C in an oven (MEMERT).

2.4 ATR-FTIR analysis

A Fourier transform infrared (FTIR) spectrometer (Nicolet iS50 FTIR) with a GladiATR single diamond attenuated total reflectance system (PIKE Technologies, Inc.) was used

to ascertain the change of functional groups and chemical bonds on the surface of raw biochar, humins-lignin biochar, and biochar-OH. Acquisitions were performed by 32 scans between 4000 and 500 cm⁻¹ at resolution 2.

2.5 Elemental analysis

Carbon and hydrogen measurements were performed on a homemade carbon/hydrogen elemental micro-analyzer (ISA, CNRS, Villeurbanne). About 1.5 mg of the sample was weighted in silver cups and dropped into a flow of 50 mL min⁻¹ of pure oxygen in a combustion unit maintained at 1050 °C half filled with CuO. Carbon and hydrogen were transformed into carbon dioxide (CO₂) and water (H₂O), before being measured using a CO₂/H₂O non-dispersive infrared detector. The precision was evaluated at $\pm 0.30\%$ for carbon and hydrogen.

Nitrogen was analyzed using a homemade nitrogen elemental micro-analyzer (ISA, CNRS Villeurbanne). The samples weighted in a silver cup were placed in a similar combustion unit as previously described where nitrogen was converted into nitrogen oxide in a flow of helium and oxygen. The gases passed through a copper wire tube maintained at 450 °C where nitrogen oxide was reduced into nitrogen N₂, and CO₂/H₂O was subsequently trapped. The resulting N₂ was quantified using a TCD Thermo Conductivity Detector. Precision was established at $< 0.20\%$.

Sulfur content was determined using a carbon sulfur SC144 analyzer (LECO, St Joseph, USA). About 10 mg of the sample was introduced in a horizontal combustion unit maintained at 1350 °C where carbon and sulfur were converted into CO₂ and SO₂ before being quantified using CO₂ and SO₂ non-dispersive infrared cells. Precision of the sulfur analysis was evaluated at 0.10%.

The O content was calculated by the difference between 100 and the sum of C, H, N, and S.

2.6 Textural analysis of biochar

Scanning electronic microscopy (SEM) analyses were performed using a Tescan Vega 3 XMU SEM X-MaxN (Oxford Instruments). Prior to observation, the biochar samples were mounted on a SEM stub and coated with platinum (3 nm). The specific surface area and pore volume were measured using a nitrogen adsorption/desorption method and an AGI-TENT Analyzer apparatus from Micromeritics (3FLEX Surface Characterization).

2.7 Adsorption experiments

MB was used as a model to investigate the adsorption capacity of biochar, humins-lignin biochar, and biochar-OH and the different interactions involved during the adsorption

process. An adequate mass of each solid was placed in a 50-mL polypropylene tube containing 40 mL of MB. Each adsorption experiment was replicated three times. Solid–liquid ratios were 7.5 g L^{-1} for biochar and 1.25 g L^{-1} for biochar-OH and humins-lignin biochar. These ratios were different considering the different adsorption capacities of each biochar and were adapted in order that MB initial concentration was kept below its solubility limit, all along adsorption experiments.

The pH of the suspensions was fixed, when necessary, by adding diluted HNO_3 or NaOH solutions. After adsorption, samples were centrifuged at 5000 rpm using a Sigma 3-30 K centrifuge and then filtered through $0.45\text{-}\mu\text{m}$ acetate filter. MB remaining in the solution was determined using a Shimadzu UV-1800 double-beam UV–visible spectrophotometer at the wavelength of 660 nm, corresponding to the maximum absorbance wavelength for MB monomers in aqueous solution. The adsorption capacity was determined using Eq. 1:

$$Q = \frac{(C_i - C_f) \times v}{m} \quad (1)$$

where Q is the adsorption capacity in mg g^{-1} , c_i (mg L^{-1}) and c_f (mg L^{-1}) are the initial and final concentrations of MB, respectively, v (L) is the volume of the solution, and m (g) is the mass of solid.

2.7.1 Kinetics adsorption experiments

For the kinetics adsorption experiments, the initial concentrations of MB were 10 mg L^{-1} for raw biochar and 50 mg L^{-1} for humins-lignin biochar and biochar-OH. The experiments were carried out at neutral pH and the contact time between MB and adsorbents ranged from 5 to 240 min. Independent experiments were carried out for each contact time. The experiments were performed in triplicate to ensure reproducibility.

2.7.2 Effect of pH

For raw biochar, the initial conditions were as follows: MB initial concentration of 10 mg L^{-1} , and 50 mg L^{-1} for humins-lignin biochar and biochar-OH. The pH value was set by adding microvolumes of diluted HNO_3 or NaOH solution in order to obtain a pH variation ranging from 2 to 10. The contact time corresponded to the equilibrium time previously determined by the kinetics experiment.

2.7.3 Effect of ionic strength

The effect of ionic strength was examined in the presence of monovalent NaCl and divalent CaCl_2 salts for modified

biochar. The test was carried out at neutral pH with the following initial salt concentrations: 0.005 M, 0.01 M, and 0.1 M. The initial concentration of MB was fixed at 50 mg L^{-1} and the contact time corresponded to the time necessary to reach adsorption, previously determined by the kinetics experiment.

2.7.4 Adsorption isotherms

The initial concentration of MB varied from 30 to 200 mg L^{-1} for NaOH -biochar, from 20 to 100 mg L^{-1} for lignin-biochar, and from 10 to 100 mg L^{-1} for raw biochar. The adsorption time corresponded to the equilibrium time determined by the kinetics study. The experiments were carried out at a neutral pH.

3 Results and discussion

3.1 Characterization of biochar

FTIR patterns are presented in Fig. 1. The main bands of raw biochar were identified at 1705, 1587, and 1134 cm^{-1} and corresponded respectively to carbonyl or carboxylic groups, $\text{C}=\text{C}$ of aromatic skeleton, and ether groups. The peaks appearing at 1016 and 739 cm^{-1} corresponded respectively to the stretching vibration of $\text{C}-\text{O}$ and the $\text{C}-\text{H}$ binding of the aromatic structure [27, 28]. After incorporation of lignin, these bands were shifted to 1701, 1589, 1136, 1019, and 780 cm^{-1} . Additional peaks were observed for lignin-biochar at 3350 cm^{-1} and 2913 cm^{-1} , which corresponded respectively to OH of alcoholic or phenolic groups and carbon sp^3 . Other new peaks appeared at 1500, 1447, and 1382 cm^{-1} , which can be assigned respectively to the $\text{C}-\text{H}$ binding of the aromatic structure, the $\text{O}-\text{CH}_3$ methoxy group, and the carboxylic group [19, 27–29]. Activation of biochar by NaOH led to significant changes in the IR pattern: two sharp peaks at 1560 cm^{-1} and 1346 cm^{-1} appeared, corresponding to carboxylate and alcoholic groups respectively [30, 31]. Formation of carboxylate and alcoholic groups had been previously observed on lignocellulosic and biochar materials modified by NaOH [32, 33].

The elemental analysis from Table 1 showed a significant increase in O content after modification by lignin and NaOH . On one hand, introduction of lignin during biochar preparation increased the number of oxygen functional groups on the surface since lignin was not degraded during thermal treatment. On the other hand, treatment with NaOH allowed to clean up the partially blocked pores of biochar, to enhance the surface porosity and increase the number of available oxygen functional groups on the surface [34, 35]. The carbon content decreased after incorporation of lignin and NaOH into the biochar structure, while the H content increased

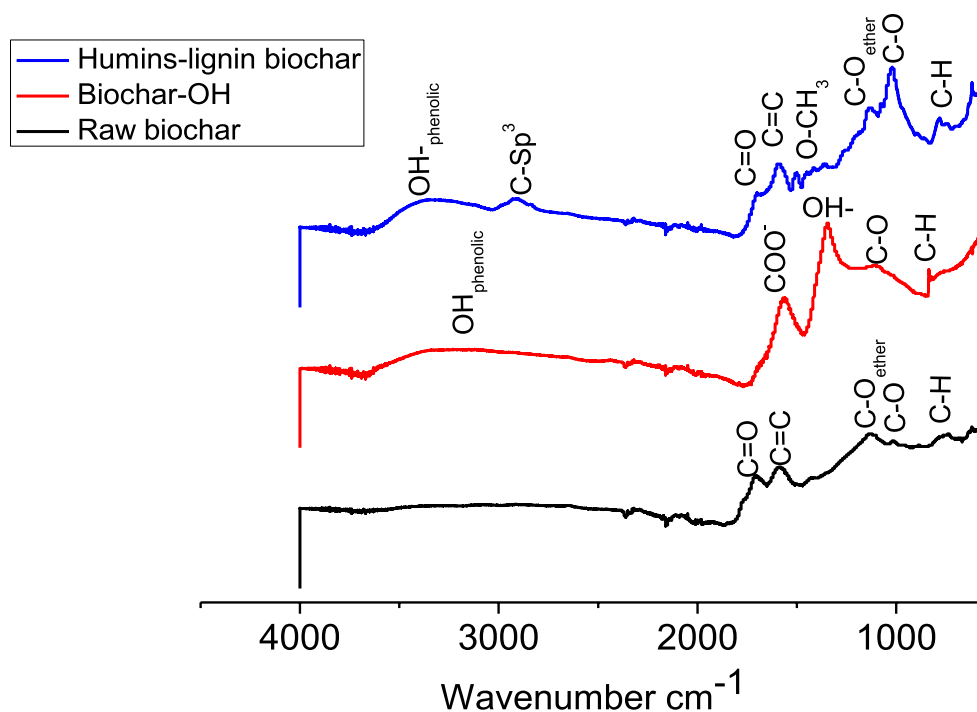


Fig. 1 IR patterns of unmodified and modified biochar

Table 1 Elementary analysis of unmodified and modified biochar

Sample	C (%)	H (%)	N (%)	S (%)	O (%)
Raw biochar	67.2	2.94	0.08	0.32	29.3
Humins-lignin biochar	55.5	4.86	0.06	1.45	38.0
Biochar-OH	57.6	3.44	1.08	<0.30	37.5

by $\approx 2\%$ and 0.5% after modification by lignin and NaOH, respectively. The hydrogen increase in modified biochar signals the formation of carboxylic and alcoholic groups on the surface. N content was negligible in raw biochar and humins-lignin biochar, whereas in biochar-OH, 1.08% of N was found. Sulfur was present in low quantity in raw biochar and biochar-OH ($\approx 0.30\%$), while humins-lignin biochar exhibited the highest sulfur content ($\approx 1.45\%$).

SEM pictures revealed a rough surface for raw biochar with the presence of some microcracks (Fig. 2a). After incorporation of lignin into the biochar, the surface became smooth and the microcracks disappeared (Fig. 2b). Concerning biochar-OH, a large presence of pits and holes appeared on the surface (Fig. 2c) which may constitute additional sites in which MB could be adsorbed. The majority of these holes were characterized by a cylindrical shape with a width ranging from 1 to $2.5\ \mu\text{m}$. Considering that the MB molecule presents dimensions of $17\ \text{\AA} \times 7.6\ \text{\AA} \times 3.25\ \text{\AA}$ [36], MB can easily accumulate inside the holes formed during NaOH treatment, regardless

of the MB molecule orientation. Figure 3a illustrates the isotherm of N_2 adsorption/desorption on raw biochar, humins-lignin biochar, and biochar-OH. Based on the classification of the International Union of Pure and Applied Chemistry (IUPAC), the shape of this isotherm is close to type 1, suggesting the presence of micropores on a solid structure. An open H4 hysteresis loop was observed for raw biochar, which is probably due to the increment in potential desorption barriers resulting from the formation of diffusion or chemical traps in the biochar [37, 38]. The SSA of raw biochar, humins-lignin biochar, and biochar-OH was determined using the BET method. As mentioned in Table 2, the specific surface area decreased from $11\ \text{m}^2\ \text{g}^{-1}$ for raw biochar to $1.04\ \text{m}^2\ \text{g}^{-1}$ for biochar-OH and to $0.33\ \text{m}^2\ \text{g}^{-1}$ for humins-lignin biochar. The pore size distribution diagram (Fig. 3b) showed the predominance of micropores on the raw biochar. The total pore volume (TPV) of raw biochar is $5.8 \cdot 10^{-3}\ \text{cm}^3\ \text{g}^{-1}$. The porosity of this material decreased dramatically after modification of the surface, particularly for humins-lignin biochar which exhibited the lowest total pore volume (TPV): $3.8 \cdot 10^{-4}\ \text{cm}^3\ \text{g}^{-1}$ (see Table 2). The decrease in the TPV in the presence of lignin indicated that lignin was well scattered on the biochar surface and occupied the majority of micropores and consequently prevented N_2 from gaining access inside the pores. Concerning biochar-OH, the TPV was $\sim 8.1 \cdot 10^{-4}\ \text{cm}^3\ \text{g}^{-1}$. This low TPV compared to raw biochar was probably related to the presence of Na^+

Fig. 2 SEM of unmodified and modified biochar. **a** Raw biochar. **b** Humins-biochar lignin. **c** Biochar-OH

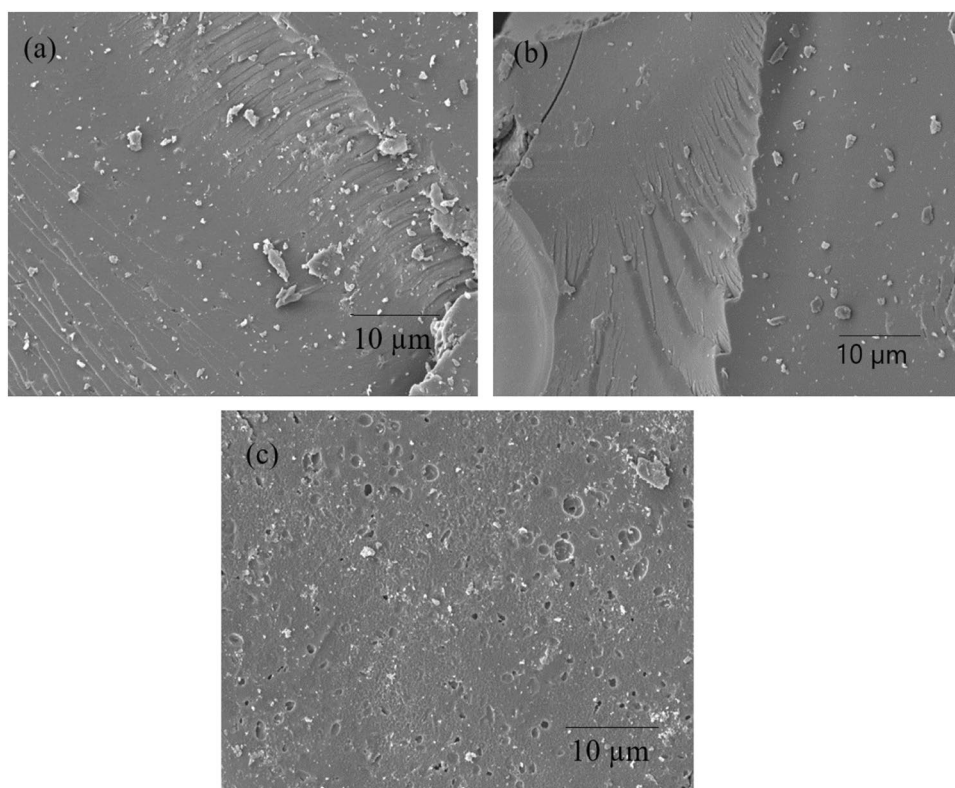


Fig. 3 N₂ adsorption/desorption isotherm (a) and pore size distribution using BJH method analysis (b)

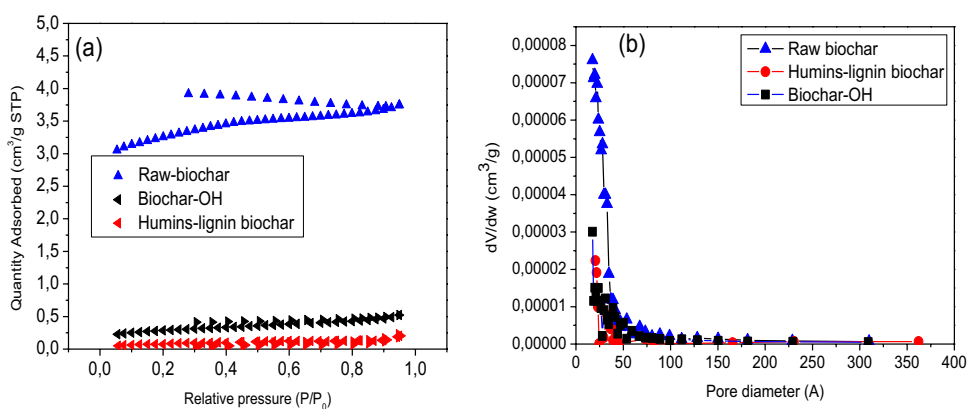


Table 2 Specific surface area and porosity of unmodified and modified biochar

Sample	S_{BET} ($\text{m}^2 \text{g}^{-1}$)	TPV ($\text{cm}^3 \text{g}^{-1}$)
Raw biochar	11	$5.8 \cdot 10^{-3}$
Humins-lignin biochar	0.33	$3.8 \cdot 10^{-4}$
Biochar-OH	1.04	$8.1 \cdot 10^{-4}$

and the type of oxygen group induced by NaOH, which blocked the micropores present on the surface, limiting accessibility of N₂ [35, 39].

3.2 Kinetics study

The adsorption kinetics of MB on unmodified and modified biochar was investigated. As seen in Fig. 4, raw biochar showed the lowest adsorption capacity. Its maximum adsorption capacity was reached after 180 min and was around 1.23 mg g^{-1} . Modification of the biochar surface noticeably improved its adsorption capacity. Humins-lignin biochar and biochar-OH exhibited a much higher MB adsorption capacity, which rapidly increased with time. Within 60 min, the MB adsorption capacity of humins-lignin biochar reached 26.719 mg g^{-1} , whereas biochar-OH removed the majority of MB from the liquid phase (93%) within the first 30 min

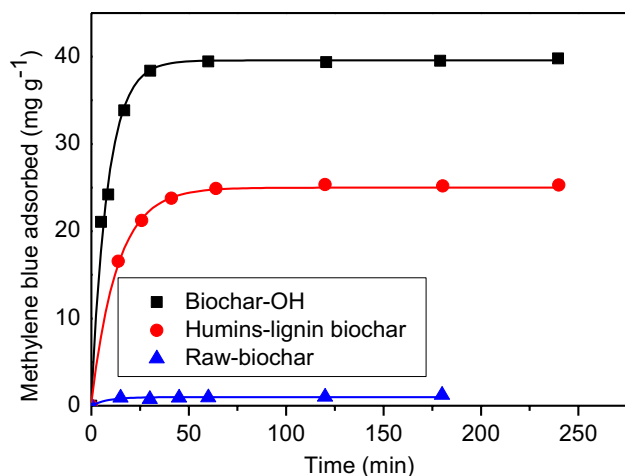


Fig. 4 Kinetics plot of MB adsorption onto unmodified and modified biochar

with an adsorption capacity of 37.316 mg g^{-1} . The trend of adsorption kinetics found in the present work is similar to previous studies concerning the removal of cationic dyes from the surface of carbonaceous materials [40–42]. MB removal occurred rapidly in the initial stage of the adsorption process, and then became relatively constant confirming the saturation of adsorbent surface sites. Modification of the biochar surface with lignin and NaOH enhanced the adsorption capacity by introducing reactive functional polar groups such as carboxylic, carbonyl, hydroxyl, and ether groups detected previously by FTIR (Fig. 1). These reactive sites could immobilize dye molecules on the biochar surface through specific bonding [43]. Biochar-OH possesses in addition to these functional groups a large quantity of macroscopic holes and pits due to alkaline treatment. These holes can increase the retention of MB by pore filling and thus contribute in a complementary way together with the chemical interactions via the functional groups in adsorption sites of biochar-OH.

Modeling of adsorption kinetics may be helpful to understand the adsorption mechanism. It is often recommended to use several models when studying adsorption on heterogeneous surfaces because the adsorption rate is often controlled by several phenomena. In the present work, three kinetics models were used: the pseudo-first-order model (PFO), the pseudo-second-order model (PSO), and intraparticle diffusion. The PFO model was initially introduced by Lagergren [44] and corresponds to the following equation:

$$\frac{dq_t}{dt} = k_1(q_e - q_t) \quad (2)$$

where k_1 (min^{-1}) is the pseudo-first-order rate constant, and q_e and q_t are the adsorption quantity (mg g^{-1}) at equilibrium

time and at t (min). A linear form of this model is expressed as follows [45]:

$$\ln(q_e - q_t) = \ln q_e - k_1 t \quad (3)$$

The PFO model assumes that the adsorption rate is related to the number of free sites on the adsorbent surface, and it was reported to be applicable when the adsorption processes are controlled by polarization-based physisorption [46, 47]. Figure 5a presents the linear plot of the PFO model for raw biochar, biochar lignin, and biochar-OH. The quality of the modeling was poor for raw biochar and biochar-OH for all time ranges, which means that the PFO model is not applicable for these adsorbents. Concerning humins-lignin biochar, the PFO model was efficient in modeling kinetics data especially in the initial stage of the adsorption process, suggesting that polarity-dependent binding occurred in the system, probably by weak Van der Waals interactions and/or π -stacking between the functional groups of humins-lignin biochar and MB molecules. The kinetic parameters calculated using the PFO model are listed in Table 3. The correlation coefficient R^2 ranged from 0.62 to 0.95 and the calculated adsorption capacities were far different from those inferred by the observed plateau for long contact times in Fig. 4.

The PSO model was reassessed by Ho and McKay in 1999 [45]. After studying several solid/liquid systems published earlier based on the PFO model, the authors reported that the PSO model was more suitable for systems in which chemisorption was the limiting rate controlling the adsorption mechanism.

The mathematical formula for the pseudo-second-order model can be represented as follows:

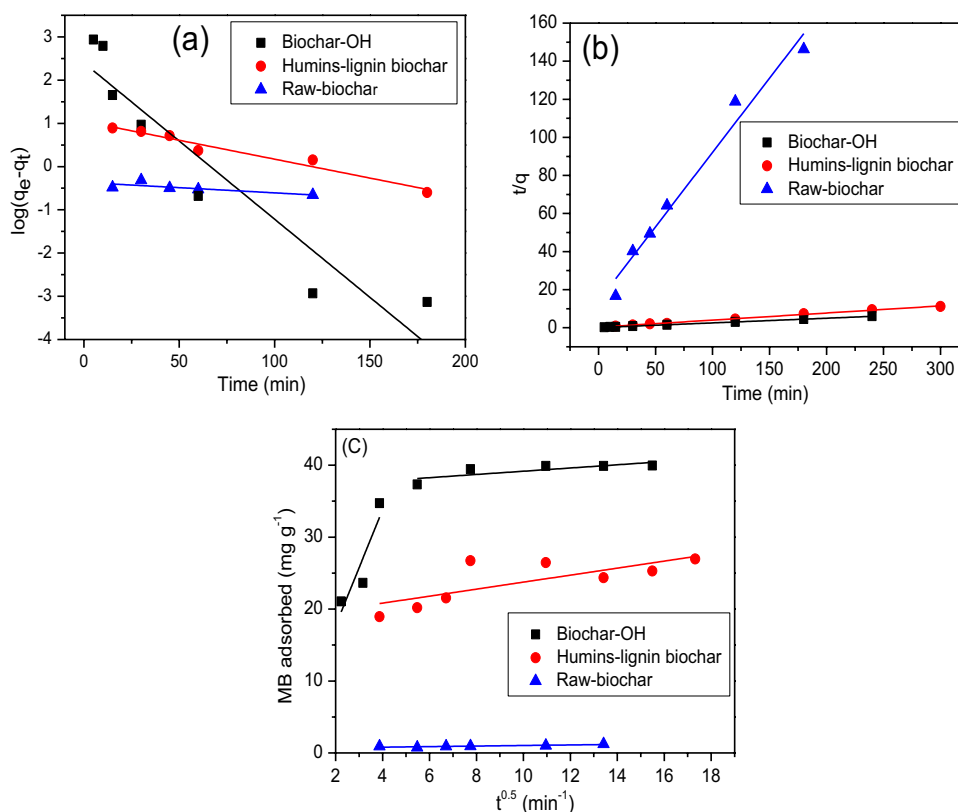
$$\frac{t}{qt} = \frac{t}{q_e} + \frac{1}{k_2 q_e^2} \quad (4)$$

where k_2 is the rate constant of the pseudo-second-order model ($\text{g mg}^{-1} \text{min}^{-1}$).

The PSO model presented in Fig. 5b showed a good fit with the adsorption data compared to the pseudo-first-order model for the three solids and all time ranges. The correlation coefficient and other parameters deduced from the PSO model are summarized in Table 4 and confirm the ability of PSO to model experimental data. R^2 is in the 0.97–0.99 range. The adsorption capacity calculated by pseudo-second-order was close to the experimental adsorption capacity inferred from the plateau in Fig. 4. These results may indicate that chemisorption was the main process involved in the adsorption mechanism.

The intraparticle diffusion model was expressed by Weber and Morris [48] as follows:

Fig. 5 Pseudo-first-order model (a), pseudo-second-order model (b), and intraparticle diffusion model (c)



$$q_t = k_3 t^{0.5} + C \quad (5)$$

where k_3 is the intraparticle diffusion rate ($\text{mg g}^{-1} \text{min}^{-1}$), and C is a constant related to the boundary layer thickness. The intraparticle diffusion model supposes that diffusion is the rate-limiting step controlling the adsorption mechanism. A linear form of plot $q_t = f(t^{0.5})$ passing through the origin may signify that the only step controlling the adsorption process is intraparticle diffusion, while a multilinear dependence may indicate that several steps describe the adsorption process. According to Fig. 5c, raw biochar and humins-lignin biochar showed a nonlinear behavior, suggesting that the adsorption process was not governed by intraparticle diffusion. This observation was supported by the low regression coefficient R^2 given in Table 3, while for biochar-OH, two straight lines on plot $q_t = f(t^{0.5})$ can depict the data, suggesting that the adsorption process takes place in two main steps. Initially, MB molecules could be transferred from the solution to the external surface of the adsorbent, forming a liquid film by diffusion. Then, in a second stage MB molecules could be diffused inside the adsorbent pores [49]. The initial stage of the adsorption process was faster than the second one, meaning that migration of MB molecules from the external surface to the pore core occurred gradually. This observation was confirmed by the constant rate value of the initial stage k'_3 which was much higher than the diffusion rate of the second stage k''_3 (Table 3). The limited transport

of MB molecules inside the pores caused an increase in the liquid film layer or the thickness of the boundary layer, which is in agreement with the increase in C over time ($C_1 < C_2$) [50]. The suitability of the intraparticle diffusion model for biochar-OH is consistent with its morphology. As seen in Fig. 2, macropores are widely distributed on the surface of biochar-OH; the pore-filling mechanism therefore presumably participated in MB adsorption.

3.3 Effect of pH on adsorption

Figure 6 shows the evolution of MB adsorption in the pH range from 2 to 10. Adsorption of MB on raw biochar was very low ($< 2.5 \text{ mg g}^{-1}$) and influence of pH was not remarkable. Removal of MB by biochar-OH was much more important than for raw biochar and ranged from 35 to 40 mg g^{-1} between pH 3 and 10. The influence of pH in MB adsorption was not significant between pH 3 and 10, but it was more significant between pH 2 and 3, with an adsorption increase from 27 to 35 mg g^{-1} . The shape of the adsorption curve on humins-lignin biochar denoted a higher pH dependency of MB adsorption on this kind of solid from pH 2 to pH 10. Removal of MB increased from 21.4 mg g^{-1} at pH = 2 to 39.2 mg g^{-1} at pH = 10. This pH dependency can be related to the deprotonation of oxygen functional groups (carboxylic, phenolic) previously detected by FTIR. As the pH increased, the deprotonation of these functional

Table 3 Parameters kinetics for methylene blue removal

Sample	Pseudo-first-order kinetic model			Pseudo-second-order kinetic model			Intraparticle diffusion model						
	Q_{exp} ($mg\ g^{-1}$)	K_1 (min^{-1})	q_e ($mg\ g^{-1}$)	R^2	K_2 ($g\cdot mg^{-1}\cdot min^{-1}$)	q_e ($mg\ g^{-1}$)	R^2	K_3' ($mg\ g^{-1}\ min^{-1}$)	C_1	R^2	K_3'' ($mg\ g^{-1}\ min^{-1}$)	C_2	R^2
Raw-biochar	1.23	$2.4\ 10^{-3}$	0.46	0.62	23.0	1.28	0.97	0.03	0.64	0.69	-	-	-
Humins-lignin biochar	25.5	$0.9\ 10^{-3}$	14.3	0.95	$8.4\ 10^{-3}$	25.7	0.99	0.48	18.87	0.53	-	-	-
Biochar-OH	39.9	$3.62\ 10^{-2}$	250.6	0.89	$6.3\ 10^{-3}$	40.8	0.99	8.06	1.56	0.66	0.22	36.9	0.69

Table 4 Zeta potential of unmodified and modified biochar and the desorption rate of methylene blue at different adsorption pH

Samples	pH	Zeta potential (mV)	Desorption rate (%)
Raw biochar	2	-11.8	3.92
	5	-49.2	16.0
	7	-50.2	16.1
	10	-51.6	14.5
Humins-lignin biochar	2	+0.43	2.98
	5	-26.1	6.07
	7	-36.4	6.09
	10	-50.6	7.02
Biochar-OH	2	-23.3	3.5
	5	-29	5.64
	7	-32.8	11.3
	10	-30.8	12.1

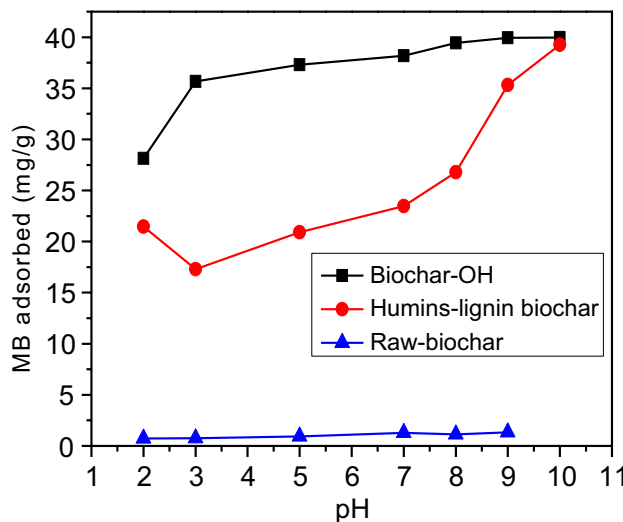


Fig. 6 Effect of pH on the adsorption of MB onto raw-biochar, biochar-lignin, and biochar-OH

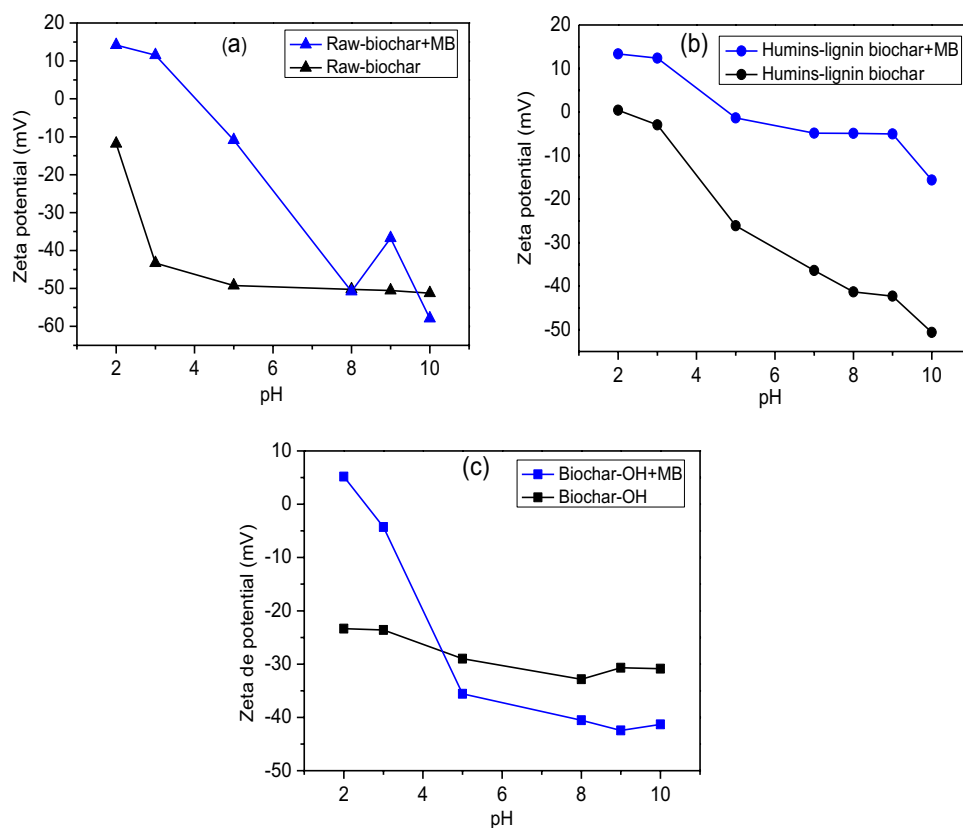
groups increased and favored electrostatic or intermolecular attraction of MB molecules [24, 51]. In order to evaluate the impact of electrostatic interaction on the adsorption process, the adsorbed MB was replaced by un-buffered salt $NaNO_3$ (1 M). It is well known in colloidal chemistry that the ions adsorbed via electrostatic interaction can be desorbed by un-buffered ion [52]. Table 4 summarizes the desorption rate of MB with an adsorption pH of 2, 5, 7, and 10. The desorption rate of MB on raw biochar was low at $pH=2$ (around $\approx 4\%$) and it increased markedly from $pH=5$ where it reached a maximum of 16% and stayed relatively constant at a neutral and basic pH. The increase in the desorption rate with the pH means that the electrostatic interaction was more important at a high pH, which is consistent with the surface charge of raw biochar. As seen in Table 4, the zeta

potential of raw biochar was -11.8 mV at $\text{pH}=2$ and shifted to highly negative values of -49.2 , -50.2 , and -51.6 mV respectively for $\text{pH}=5$, 7 , and 10 . For humins-lignin biochar and biochar-OH, the desorption rate was lower, with an increase ranging from $\approx 3\%$ at $\text{pH}=2$ to 7% at $\text{pH}=10$ for humins-lignin biochar and from 3.5% at $\text{pH}=2$ to 12% at $\text{pH}=10$ for biochar-OH.

In order to elucidate the non-electrostatic interaction occurring during MB adsorption, zeta potential measurements were performed as a function of pH before and after MB adsorption. This parameter indicates the potential difference between the diffusion layer and the stationary layer strongly attached to the particle surface. In other words, the measure of zeta potential gives the electrical potential at the edge of the diffuse layer, which is an area called the slipping plane. Thereby, only ions adsorbed by molecular interaction on the surface have an impact on the zeta potential magnitude, and consequently, electrostatic adsorption of ions was not considered because the adsorbed ions are localized in the diffuse layer [53]. Figure 7a shows that the surface charge of raw biochar was negative whatever the pH value in the absence of MB. It decreased abruptly from -11.8 mV at $\text{pH}=2$ to -49.2 mV at $\text{pH}=5$ where it finally reached a plateau. This behavior can be explained by the ionization of oxygen functional groups (carboxyl for example) previously identified on the raw biochar surface by

FTIR (Fig. 1). The negative sites present on the surface even at low pH constituted available sites for positively charged MB molecules. After adsorption of MB, the surface charge shifted to positive values in acidic pH ($\sim 2\text{--}3$) proving that MB transferred its positive charge on the surface, and probably that intermolecular bindings were formed between MB molecules and the functional groups on the adsorbent surface. At basic pH , an unexpectedly high negative charge developed on the surface after MB adsorption despite almost complete adsorption of MB (around $96\text{--}99\%$). The surface charges after MB adsorption turned negative with a magnitude close or equal to the magnitude of the surface charge before adsorption. This behavior is probably related to the orientation of MB molecules. The high negative charge density on raw biochar constrains the orientation of MB molecules in a tilted fashion [54]. This type of orientation tends to favor the aggregation of MB molecules and it probably causes a heterogenous distribution of MB molecules on the adsorbent surface, consequently reducing the impact of the positive cationic charge. Furthermore, the aggregated molecules bind to raw biochar through electrostatic interactions, which are not measured by zeta potential. This result is consistent with the desorption rate, which demonstrates the contribution of electrostatic interactions to MB adsorption. Therefore, OH^- fixed on the Stern layer and the deprotonated oxygen functional surface groups probably controls

Fig. 7 Zeta potential of raw-biochar (a), humins-lignin biochar (b), and biochar-OH (c) before and after MB adsorption



the zeta potential value to a large extent, which explains the negative charge maintained on the surface after MB adsorption in an alkaline medium.

Figure 7b illustrates the evolution of the zeta potential of humins-lignin biochar as a function of the pH before and after MB adsorption. In the absence of MB, humins-lignin biochar exhibits a point of zero charge at pH = 2 confirming the incorporation of lignin into the biochar structure. As reported previously, lignin is characterized by a point of zero charge around pH = 2 [55, 56]. The surface charge decreased gradually with the pH increase until it reached -50.6 mV at pH = 10, which was related to the deprotonation of the alcoholic and carboxylic groups previously detected by FTIR on humins-lignin biochar. After adsorption of MB, the surface charge shifted to positive values at pH = 2 and 3, whereas from pH = 5 to 10, the surface charge ranged from -1.37 to -15.6 mV. The increase in the surface charge after MB adsorption is attributed to the attachment of positively charged MB molecules on the adsorbent surface through intermolecular interactions. The variation in the biochar-OH surface charge depending on the pH is represented in Fig. 7c. Before MB adsorption, the surface charge was negative for the whole pH range. It decreased with the pH, from -23.3 mV at pH = 2 to -30.8 mV at pH = 10. Compared with raw biochar and humins-lignin biochar, the surface charge of biochar-OH decreased slightly with the pH increase (variation of only -7.5 mV). Activation of biochar by NaOH probably resulted in the formation of some hydroxyl or phenolic hydroxyl groups characterized by high pKa values, which consequently could not be ionized in the pH range of 2–10 [57]. After MB adsorption, the surface charge increased noticeably at very low pH, especially at pH = 2 where it exhibited a positive value related to direct attachment of positively charged MB molecules. However, from pH = 5, the surface charge decreased unexpectedly and became relatively steady at pH = 8 ($\zeta = -40.5$ mV). Despite the noticeable improvement of the adsorption capacity from pH = 5, the contribution of the positive charge of MB on the surface of biochar-OH was not noticed. There was probably a strong restructuring of OH⁻ ions after fixation of MB in a basic medium.

3.4 Effect of ionic strength on MB adsorption

Dye effluents discharged by the textile industry contain a significant amount of salts. Hence, the influence of salts on MB adsorption should be studied. Figure 8 shows the variation in MB adsorption as a function of salt concentration. Two types of salts were used in the present work, NaNO₃ and CaCl₂, to examine the competitive effect of monovalent and divalent ions. The increase in salt concentration inhibited the removal of MB by humins-lignin biochar and biochar-OH. MB removal by humins-lignin biochar decreased by 12% and 35%

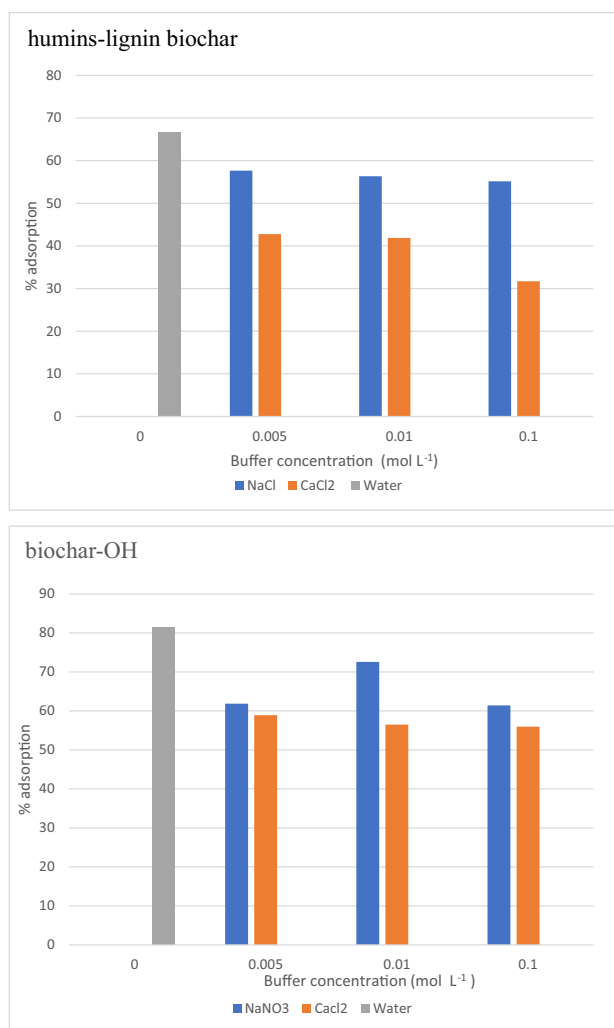


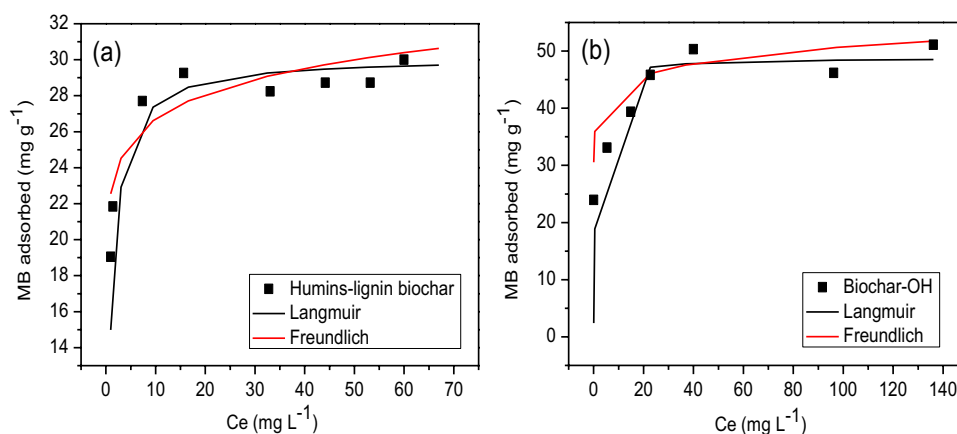
Fig. 8 Effect of sodium nitrate and calcium chloride on MB adsorption onto humins-lignin biochar and biochar-OH

with the highest concentration of NaNO₃ and CaCl₂, respectively. For MB removal by biochar-OH, a decrease of 20% and 25% was observed in the presence of NaNO₃ and CaCl₂, respectively. It was reported previously that the presence of salts during MB adsorption reduces the density of adsorbent sites by occupying or blocking the available sites. Furthermore, salts can create intermolecular repulsion between MB molecules, preventing their aggregation and consequently hinder the orientation of MB molecules that contributes to multilayer adsorption [58]. In Fig. 9, divalent ions impacted MB adsorption more than monovalent ions, which was probably related to atomic radii and atomic charge [51].

3.5 Adsorption isotherm

The Langmuir and Freundlich models were used to investigate the adsorption mechanism of MB on raw

Fig. 9 Adsorption isotherm of MB on humins-lignin biochar (a) and biochar-OH (b)



and modified biochar. The Langmuir model is based on the assumption that the adsorbent surface sites are uniformly homogeneous, and that the adsorption of solute molecules is limited to the monolayer on the surface of the adsorbent, with no interaction between molecules adsorbed on adjacent sites. The Freundlich model supposes that the adsorbent surface sites are heterogeneous and that multilayer adsorption possibly occurs during the reaction process. The mathematical formulas of the Langmuir and Freundlich models are expressed by Eqs. 6 and 7, respectively.

$$\frac{C_e}{q_e} = \frac{1}{Lq_{\max}} + \frac{C_e}{q_{\max}} \quad (6)$$

$$\ln q_e = \ln K_f + \frac{1}{n} \ln C_e \quad (7)$$

where C_e is the MB concentration at equilibrium (mg L^{-1}), L is the Langmuir constant related to the energy of adsorption (L mg^{-1}), q_{\max} is the monolayer maximum adsorption capacity (mg g^{-1}), and K_f and n are the Freundlich constants related respectively to the affinity and intensity of the adsorption process.

Figure 9 represents MB adsorption isotherms on modified biochar. The adsorption isotherm of raw biochar was not presented since its sorption efficiency was too low, and consequently, it was not possible to determine Langmuir- or Freundlich-like isotherms. In Fig. 9, the non-linear plot of the Langmuir model offered a good

fit with the experimental data compared with the Freundlich model for humins-lignin biochar and biochar-OH. Table 5 includes different parameters determined using the Langmuir and Freundlich models. The correlation coefficient of linear regression for the Langmuir model was $R^2 = 0.99$ for both humins-lignin biochar and biochar-OH, while the correlation coefficients of linear regression for the Freundlich model were 0.40 for humins-lignin biochar and 0.59 for biochar-OH. The high correlation coefficient found for the Langmuir model indicates its suitability to describe adsorption processes on modified biochar. These results suggest that MB adsorption mainly occurred in a monolayer on the adsorbent surface. The maximum adsorption capacities deduced from the Langmuir model (Table 5) were 48.78, 30.12, and 1.05 mg g^{-1} for biochar-OH, humins-lignin biochar, and raw biochar respectively. According to this finding, the surface modification using lignin and NaOH strongly enhanced the adsorption capacity of biochar (30 times and 50 times, respectively). The adsorption capacity exhibited by modified biochar was comparable with various adsorbents derived from different sources (Table 6). Therefore, both biochar-OH and humins-lignin biochar can be used as low-cost adsorbents for the removal of cationic dye from wastewater.

3.6 Possible surface interaction

In order to elucidate the different interactions occurring during MB adsorption on biochar and modified biochar, FTIR

Table 5 Parameters of Langmuir and Freundlich models for methylene blue removal

Samples	Langmuir model			Freundlich model		
	q_{\max} (mg g^{-1})	L (L mg^{-1})	R^2	K_f	$1/n$	R^2
Raw biochar	1.05	0.36	0.67	-	-	-
Humins-lignin biochar	30.12	1.04	0.99	22.64	0.07	0.40
Biochar-OH	48.78	1.29	0.99	37.63	0.06	0.59

Table 6 Comparison of adsorption capacity of different adsorbents for MB removal

Adsorbents	Maximal adsorption capacity (mg g ⁻¹)	References
Kenaf fiber char	22.7	[67]
Nut shell activated carbon	5.3	[68]
Wheat straw biochar	12.03	[69]
Wood apple shell activated carbon	37	[70]
Sludge-rice husk biochar	22.59	[53]
Raw avocado seeds	99.83	[58]
Sludge and tea waste	12.57	[62]
Sludge-derived biochar	24.10	[71]
Lignin derived from spent coffee grounds	66.22	[72]
Biochar-OH	48.78	This study
Humins-lignin biochar	30.12	This study

patterns were interpreted before and after MB adsorption and presented in the supplementary data (Fig. S1). Table 7 summarizes the main bands involved in the adsorption process. The spectrum of raw biochar did not exhibit a noticeable change after MB adsorption. The only change concerned the characteristic peak of aromatic C=C appearing at 1587 cm⁻¹ in raw biochar which was shifted after adsorption to 1575 cm⁻¹ suggesting involvement of π - π interactions

between the aromatic structure of raw biochar and the MB aromatic ring. The absence of noticeable change on the FTIR pattern after MB adsorption means that chemisorption contributes only marginally to the adsorption process. π - π interaction promotes self-association of MB molecules and formation of H-aggregates of MB [59, 60], which in their turn link to the adsorbent surface via a physisorption mechanism. π - π interaction was also supposed to be involved in the adsorption of MB by humins-lignin biochar. The stretching vibrations of aromatic C=C at 1589 cm⁻¹ were shifted to 1594 cm⁻¹ after MB adsorption [21, 61]. The peak at 1382 cm⁻¹ assigned to COOH was shifted to 1358 cm⁻¹ suggesting formation of hydrogen bonds with the amino group of the MB molecule [62]. This proposition was supported by the emergence of a new peak at 1325 cm⁻¹ corresponding to terminal C-N bonds in saturated dimethylamino groups [63, 64]. The peak localized at 1136 cm⁻¹ assigned to the C—O bond of the ether groups was shifted to 1124 cm⁻¹, which probably means that the ether group was engaged in MB adsorption. A new peak appeared at 898 cm⁻¹, which probably corresponded to the C-H bond of the MB aromatic ring [53, 65]. In biochar-OH, the carboxylate COO⁻ band initially at 1560 cm⁻¹ was shifted to 1591 cm⁻¹ suggesting electrostatic interaction between the negative charge of the carboxylate group and the amino group of MB molecules. The peak at 1346 cm⁻¹ assigned to the alcohol group was shifted to 1322 cm⁻¹ after MB adsorption, suggesting

Table 7 The characteristic frequencies of FTIR bands of unmodified and modified biochar before and after methylene blue adsorption

Samples	Functional groups	Assignment			
		Before adsorption	After adsorption	Difference	Methylene blue (cm ⁻¹)
Raw-biochar	C=C aromatic	1587	1575	12	
Humins-lignin biochar	C=C aromatic	1589	1594	5	
	CO ₂ H carboxylic group	1382	1358	24	
	C-N of dimethylamine group of MB	-	1325		1328
	C-O of ether group	1136	1124	12	
	C-H of MB aromatic ring		898		872
	C sp ³	2913	2928	15	
	C-H aromatic ring	780	785	5	
Biochar-OH	Carboxylic COOH	1560	1591	31	
		1346	1322	24	
	C _{het} =N ⁺ (CH ₃) ₂	-	1691		1706
	C _{het} =S		1485		1481
	C-H		1379		1386
	(C-C) _{het}		1220		1220
	(C-H) _{het}		1168		1170
	(C-N) _{het}		1122		1126
	(C-S-C)		1029		1031
	C-H of MB aromatic ring		882		872

that the alcohol OH-group involved in the adsorption was probably established through the hydrogen bond with the $C_{\text{heterocycle}}=\text{N}^+(\text{CH}_3)_2$ functional group whose band appears at 1691 cm^{-1} [51, 66]. New peaks appeared in the range of $1400\text{--}882\text{ cm}^{-1}$, which were attributed to the functional groups of adsorbed MB molecules (Table 6) [66].

4 Conclusion

Biochar derived from humins from the biorefinery industry was produced in a one-step thermal process. The modification of biochar significantly improved MB removal. Compared to raw biochar, the adsorption capacity increased 30 times when combined with lignin and 50 times after NaOH activation. Oxygen functional groups introduced on the biochar surface after modification tended to bond with MB molecules via physical or chemical interactions, while holes and pits that widely expanded on the biochar-OH surface probably promoted MB retention via pore filling. The adsorption equilibrium was rapidly reached for modified biochar (after 30 min for biochar-OH and 60 min for humins-lignin biochar), suggesting a high affinity of MB towards the surface. The adsorption isotherms offered a good fit with the Langmuir model for biochar-OH and humins-lignin biochar, suggesting that the adsorption process occurred mainly in a monolayer on the surface with a maximum monolayer adsorption capacity of 48.78 mg g^{-1} for biochar-OH and 30.12 mg g^{-1} for humins-lignin biochar. Biochar-OH and humins-lignin biochar exhibited a promising potential to remove cationic dyes. Nevertheless, the presence of divalent competing ions (such as calcium) reduced adsorption efficiency more than monovalent ions (such as sodium), limiting the use of biochar as adsorbent to effluent with low ionic strength. Due to the weak pH dependency of adsorption on biochar-OH, it could be suitable as well for acidic or basic effluents, while humins-lignin biochar could be suitable for basic effluents. As a perspective of this work, reusability of biochar should be investigated.

Supplementary Information The online version contains supplementary material available at <https://doi.org/10.1007/s13399-022-03398-w>.

Author contribution Yassine Bentahar: conceived the idea, accomplishment of experimental tests, designed the manuscript, and wrote the manuscript.

Claire Lomenech: designed the manuscript, contribution on the interpretation of the results, and supervision of work.

Alice Mija: synthesis of biochar and humins-lignin biochar samples, FTIR analysis, correction, and revision of manuscript.

Ed de Jong: synthesis of biochar and humins-lignin biochar samples, correction, and revision of manuscript.

Erik Bonjour: realization of elemental analysis.

Patrick Jame: realization of elemental analysis.

Charlotte Hurel: supervision of work, contribution in the interpretation of results and redaction and correction of the manuscript, realization of SEM analysis.

All authors have read and approved the manuscript.

Funding This work was supported by the French government, through the UCA^{JEDI} Investments in the Future project managed by the National Research Agency (ANR) with the reference number ANR-15-IDEX-01. The scanning electron microscope of the Centre Commun de Microscopie Appliquée (CCMA) was funded by the Région Sud/Provence-Alpes-Côte d'Azur and the Conseil Départemental des Alpes Maritimes.

Data availability Not applicable.

Declarations

Ethics approval Not applicable.

Competing interests The authors declare no competing interests.

References

- Rao P, Rathod V (2019) Valorization of food and agricultural waste: a step towards greener future. *Chem Rec* 19(9):1858–1871
- Colonna S, Gaggero N, Richelmi C, Pasta P (1999) Recent biotechnological developments in the use of peroxidases. *Trends Biotechnol* 17(4):163–168
- Pan Y, Yang Y, Pang Y, Shi Y, Long Y, Zheng H (2018) Enhancing the peroxidase-like activity of ficin via heme binding and colorimetric detection for uric acid. *Talanta* 185:433–438
- Al-Mansour A, Chow CL, Feo L, Penna R, Lau D (2019) Green concrete: By-products utilization and advanced approaches. *Sustainability* 11(19):5145
- Isikgor FH, Becer CR (2015) Lignocellulosic biomass: a sustainable platform for the production of bio-based chemicals and polymers. *Polym Chem* 6(25):4497–4559
- Tosi P, van Klink G.P, Celzard A, Fierro V, Vincent L, de Jong E, Mija. (2018) A. Auto-crosslinked rigid foams derived from biorefinery byproducts. *ChemSusChem* 11(16): 2797–2809.
- De Jong E, Visser HA, Sousa Dias A, Harvey C, Gruter G-JM (2022) The road to bring FDCA and PEF to the market. *Polymers* 14:943–974
- Muralidhara A, Tosi P, Mija A, Sbirrazzuoli N, Len C, Engelen V, De Jong E, Marlair G (2018) Insights on thermal and fire hazards of humins in support of their sustainable use in advanced biorefineries. *ACS Sustainable Chem Eng* 12:16692–16701
- Kang S, Fu J, Zhang G (2018) From lignocellulosic biomass to levulinic acid: a review on acid-catalyzed hydrolysis. *Renewable Sustainable Energy Rev* 94:340–362
- Haq I, Mazumder P, Kalamdhad AS (2020) Recent advances in removal of lignin from paper industry wastewater and its industrial applications—a review. *Bioresour Technol* 312:123636
- Ragauskas AJ, Beckham GT, Biddy MJ, Chandra R, Chen F, Davis MF et al (2014) Lignin valorization: improving lignin processing in the. *Biorefinery. Science* 344(6185):1246843
- Luo H, Abu-Omar MM (2017) Chemicals from lignin. *Encyclopedia of sustainable technologies* 3:573–585
- Nayak A, Bhushan B (2019) An overview of the recent trends on the waste valorization techniques for food wastes. *J Environ Manage* 233:352–370

14. Huang Q, Song S, Chen Z, Hu B, Chen J, Wang X (2019) Biochar-based materials and their applications in removal of organic contaminants from wastewater: state-of-the-art review. *Biochar* 1(1):45–73
15. Sun Y, Wang T, Sun X, Bai L, Han C, Zhang P (2021) The potential of biochar and lignin-based adsorbents for wastewater treatment: Comparison, mechanism, and application—a review. *Ind Crops Prod* 166:113473
16. Xiang W, Zhang X, Chen K, Fang J, He F, Hu X et al (2020) Enhanced adsorption performance and governing mechanisms of ball-milled biochar for the removal of volatile organic compounds (VOCs). *Chem Eng J* 385:123842
17. Lyu H, Gao B, He F, Zimmerman AR, Ding C, Tang J, Crittenden JC (2018) Experimental and modeling investigations of ball-milled biochar for the removal of aqueous methylene blue. *Chem Eng J* 335:110–119
18. Wang X, Xing B (2007) Importance of structural makeup of biopolymers for organic contaminant sorption. *Environ Sci Technol* 41(10):3559–3565
19. Klapiszewski Ł, Nowacka M, Milczarek G, Jesionowski T (2013) Physicochemical and electrokinetic properties of silica/lignin biocomposites. *Carbohydr Polym* 94(1):345–355
20. Cho DW, Yoon K, Ahn Y, Sun Y, Tsang DC, Hou D et al (2019) Fabrication and environmental applications of multifunctional mixed metal-biochar composites (MMBC) from red mud and lignin wastes. *J Hazard Mater* 374:412–419
21. Zafar MN, Nadeem R, Hanif MA (2007) Biosorption of nickel from protonated rice bran. *J Hazard Mater* 143(1–2):478–485
22. Ye H, Zhu Q, Du D (2010) Adsorptive removal of Cd (II) from aqueous solution using natural and modified rice husk. *Bioresour Technol* 101(14):5175–5179
23. Akhtar M, Iqbal S, Kausar A, Bhangar MI, Shaheen MA (2010) An economically viable method for the removal of selected divalent metal ions from aqueous solutions using activated rice husk. *Colloids Surf. B.* 75(1):149–155
24. Mu Y, Ma H (2021) NaOH-modified mesoporous biochar derived from tea residue for methylene Blue and Orange II removal. *Chem Eng Res Des* 167:129–140
25. Islam MA, Ahmed MJ, Khanday WA, Asif M, Hameed BH (2017) Mesoporous activated coconut shell-derived hydrochar prepared via hydrothermal carbonization-NaOH activation for methylene blue adsorption. *J Environ Manage* 203:237–244
26. Tosi P, van Klink GP, Hurel C, Lomenech C, Celzard A, Fierro V, Delgado-Sanchez C, Mija A (2020) Investigating the properties of humins foams, the porous carbonaceous materials derived from biorefinery by-products. *Appl Mater Today* 20:100622
27. Stark Nicole M, Yelle Daniel J, Agarwal Umesh P. (2016). Techniques for characterizing lignin. In: *Lignin in polymer composites*. Faruk, Omar; Sain, Mohini, eds. Elsevier; Kidlington, Oxford. Chapter 4: 49–66.
28. Jiang C, Bo J, Xiao X, Zhang S, Wang Z, Yan G et al (2020) Converting waste lignin into nano-biochar as a renewable substitute of carbon black for reinforcing styrene-butadiene rubber. *Waste Manage* 102:732–742
29. Guo X, Zhang S, Shan XQ (2008) Adsorption of metal ions on lignin. *J Hazard Mater* 151(1):134–142
30. Hemmalakshmi S, Priyanga S, Devaki K (2017) Fourier transform infra-red spectroscopy analysis of *Erythrina variegata* L. *Int J Pharm Sci Res International* 9(11):2062–2067
31. Ferenc W, Bernat M, Sarzynski J, Paszkowska B (2008) The physico-chemical properties of 4-chlorophenoxyacetates of Mn (II), Co (II), Ni (II) and Cu (II). *Ecletica Quim* 33:7–14
32. Anastopoulos I, Panagiotou M, Ehaliotis C, Tarantilis PA, Massas I (2015) NaOH pretreatment of compost derived from olive tree pruning waste biomass greatly improves biosorbent characteristics for the removal of Pb²⁺ and Ni²⁺ from aqueous solutions. *Chem Ecol* 31(8):724–740
33. An Q, Miao Y, Zhao B, Li Z, Zhu S (2020) An alkali modified biochar for enhancing Mn²⁺ adsorption: performance and chemical mechanism. *Mater Chem Phys* 248:122895
34. Regmi P, Moscoso JLG, Kumar S, Cao X, Mao J, Schafran G (2012) Removal of copper and cadmium from aqueous solution using switchgrass biochar produced via hydrothermal carbonization process. *J Environ Manage* 109:61–69
35. Rizwan M, Lin Q, Chen X, Li Y, Li G, Zhao X, Tian Y (2020) Synthesis, characterization, and application of magnetic and acid modified biochars following alkaline pretreatment of rice and cotton straws. *Sci Total Environ* 714:136532
36. Arias M, López E, Nuñez A, Rubinos D, Soto B, Barral MT, Díaz-Fierros F (1999) Adsorption of methylene blue by red mud, an oxide-rich byproduct of bauxite refining. Effect of mineral-organic-microorganism interactions on soil and freshwater environments. Springer, Boston, MA, pp 361–365
37. Chen Z, Liu T, Tang J, Zheng Z, Wang H, Shao Q et al (2018) Characteristics and mechanisms of cadmium adsorption from aqueous solution using lotus seedpod-derived biochar at two pyrolytic temperatures. *Environ Sci Pollut Res* 25(12):11854–11866
38. Zhang M, Gao B (2013) Removal of arsenic, methylene blue, and phosphate by biochar/AlOOH nanocomposite. *Chem Eng J* 226:286–292
39. Li Y, Shao J, Wang X, Deng Y, Yang H, Chen H (2014) Characterization of modified biochars derived from bamboo pyrolysis and their utilization for target component (furfural) adsorption. *Energy Fuels* 28(8):5119–5127
40. Jin Y, Zeng C, Lü QF, Yu Y (2019) Efficient adsorption of methylene blue and lead ions in aqueous solutions by 5-sulfosalicylic acid modified lignin. *Int J Biol Macromol* 123:50–58
41. Fan S, Wang Y, Wang Z, Tang J, Tang J, Li X (2017) Removal of methylene blue from aqueous solution by sewage sludge-derived biochar: adsorption kinetics, equilibrium, thermodynamics and mechanism. *J Environ Chem Eng* 5(1):601–611
42. Zhang W, Mao S, Chen H, Huang L, Qiu R (2013) Pb (II) and Cr (VI) sorption by biochars pyrolyzed from the municipal wastewater sludge under different heating conditions. *Bioresour Technol* 147:545–552
43. Vyavahare GD, Gurav RG, Jadhav PP, Patil RR, Aware CB, Jadhav JP (2018) Response surface methodology optimization for sorption of malachite green dye on sugarcane bagasse biochar and evaluating the residual dye for phyto and cytogenotoxicity. *Chemosphere* 194:306–315
44. Lagergren SY (1898) Zur Theorie der sogenannten Adsorption gelöster Stoffe. *Kungliga Svenska Vetenskapsakad Handlingar* 24:1–39
45. Ho Y, McKay G (1999) Pseudo-second order model for sorption processes. *Process Biochem* 34:451–465
46. Kezerle A, Velić N, Hasenay D, Kovačević D (2018) Lignocellulosic materials as dye adsorbents: adsorption of methylene blue and Congo red on brewers' spent grain. *Croat Chem Acta* 91:53–64
47. Lee Y, Lee H, Jung D, Chen Z, Lim S (2018) Chloride ion adsorption capacity of anion exchange resin in cement mortar. *Materials* 11(4):560
48. Morris J. C, Weber JR W. J. (1964). Removal of biologically-resistant pollutants from waste waters by adsorption. In *Advances in water pollution research*. Pergamon. pp. 231–266.
49. Mortazavian S, Saber A, Hong J, Bae JH, Chun D, Wong N et al (2019) Synthesis, characterization, and kinetic study of activated carbon modified by polysulfide rubber coating for aqueous hexavalent chromium removal. *J Ind Eng Chem* 69:196–210

50. Haque ANMA, Remadevi R, Rojas OJ, Wang X, Naebe M (2020) Kinetics and equilibrium adsorption of methylene blue onto cotton gin trash bioadsorbents. *Cellulose* 27:6485–6504
51. Dawood S, Sen TK, Phan C (2016) Adsorption removal of methylene blue (MB) dye from aqueous solution by bio-char prepared from Eucalyptus sheathiana bark: kinetic, equilibrium, mechanism, thermodynamic and process design. *Desalin Water Treat* 57(59):28964–28980
52. Tong XJ, Li JY, Yuan JH, Xu RK (2011) Adsorption of Cu (II) by biochars generated from three crop straws. *Chem Eng J* 172(2–3):828–834
53. Chen S, Qin C, Wang T, Chen F, Li X, Hou H, Zhou M (2019) Study on the adsorption of dyestuffs with different properties by sludge-rice husk biochar: adsorption capacity, isotherm, kinetic, thermodynamics and mechanism. *J Mol Liq* 285:62–74
54. Bujdák J, Iyi N, Kaneko Y, Sasai R (2003) Molecular orientation of methylene blue cations adsorbed on clay surfaces. *Clay Miner* 38(4):561–572
55. Berrima B, Maatar W, Mortha G, Boufi S, El Aloui L, Belgacem M (2016) Adsorption of heavy metals on charcoal from lignin. *Cellul Chem Technol* 50:701–709
56. Wu Y, Zhang S, Guo X, Huang H (2008) Adsorption of chromium (III) on lignin. *Bioresour Technol* 99(16):7709–7715
57. Jiang C, He H, Jiang H, Ma L, Jia D. M. (2013). Nano-lignin filled natural rubber composites: preparation and characterization. *eXPRESS Polym. Lett*, 7(5) : 480–493
58. Dhaouadi F, Sellaoui L, Dotto GL, Bonilla-Petriciolet A, Erto A, Lamine AB (2020) Adsorption of methylene blue on comminuted raw avocado seeds: interpretation of the effect of salts via physical monolayer model. *J Mol Liq* 305:112815
59. Nie S, Zhang Y, Liu B, Li Z, Hu H, Xue G et al (2010) Two inorganic–organic hybrid materials based on polyoxometalate anions and methylene blue: Preparations, crystal structures and properties. *J Solid State Chem* 183(12):2957–2962
60. Li Q, An X, Gong B, Cheng J (2008) Spectroscopic and theoretical evidence for the cooperativity between red-shift hydrogen bond and blue-shift hydrogen bond in DMSO aqueous solutions. *Spectrochim Acta, Part A* 69(1):211–215
61. Zhang Y, Zheng Y, Yang Y, Huang J, Zimmerman AR, Chen H et al (2021) Mechanisms and adsorption capacities of hydrogen peroxide modified ball milled biochar for the removal of methylene blue from aqueous solutions. *Bioresour Technol* 337:125432
62. Fan S, Tang J, Wang Y, Li H, Zhang H, Tang J et al (2016) Biochar prepared from co-pyrolysis of municipal sewage sludge and tea waste for the adsorption of methylene blue from aqueous solutions: kinetics, isotherm, thermodynamic and mechanism. *J Mol Liq* 220:432–441
63. Grumelli D, Mendez De Leo LP, Bonazzola C, Zamlyny V, Calvo EJ, Salvarezza RC (2010) Methylene blue incorporation into alkanethiol SAMs on Au (111): effect of hydrocarbon chain ordering. *Langmuir* 26(11):8226–8232
64. Zhang D, Fu L, Liao L, Liu N, Dai B, Zhang C (2012) Preparation, characterization, and application of electrochemically functional graphene nanocomposites by one-step liquid-phase exfoliation of natural flake graphite with methylene blue. *Nano Res* 5(12):875–887
65. Sahu S, Pahi S, Tripathy S, Singh SK, Behera A, Sahu UK, Patel RK (2020) Adsorption of methylene blue on chemically modified lychee seed biochar: dynamic, equilibrium, and thermodynamic study. *J Mol Liq* 315:113743
66. Ovchinnikov OV, Evtukhova AV, Kondratenko TS, Smirnov MS, Khokhlov VY, Erina OV (2016) Manifestation of intermolecular interactions in FTIR spectra of methylene blue molecules. *Vib Spectrosc* 86:181–189
67. Yener T, Kopac G, Dogu T, Dogu. (2008) Dynamic analysis of sorption of Methylene Blue dye on granular and powdered activated carbon. *Chem Eng J* 144:400–406
68. Ragupathy S, Raghu K, Prabu P (2015) Synthesis and characterization of TiO₂ loaded cashew nut shell activated carbon and photocatalytic activity on BG and MB dyes under sunlight radiation. *Spectrochim. Acta Part A Mol Biomol Spectrosc* 138:314–320
69. Liu Y, Zhao X, Li J, Ma D, Han R (2012) Characterization of bio-char from pyrolysis of wheat straw and its evaluation on methylene blue adsorption. *Desalin Water Treat* 46:115–123
70. Malarvizhi R, Sulochana N (2008) Sorption isotherm and kinetic studies of methylene blue uptake onto activated carbon prepared from wood apple shell. *J Environ Prot Sci* 2:40–44
71. Fan S, Wang Y, Wang Z, Tang J, Tang J, Li X. (2017). Removal of methylene blue from aqueous solution by sewage sludge-derived biochar Adsorption kinetics equilibrium thermodynamics and mechanism. *J Environ Chem Eng*.5(1) 601 611
72. Taleb F, Ammar M, ben Mosbah M, ben Salem R, Moussaoui Y. (2020) Chemical modification of lignin derived from spent coffee grounds for methylene blue adsorption. *Sci Rep* 10(1):1–13

Publisher's note Springer Nature remains neutral with regard to jurisdictional claims in published maps and institutional affiliations.

Springer Nature or its licensor holds exclusive rights to this article under a publishing agreement with the author(s) or other rightsholder(s); author self-archiving of the accepted manuscript version of this article is solely governed by the terms of such publishing agreement and applicable law.